



# The efficiency of recycled glass powder in mitigating the alkali-silica reaction induced by recycled glass aggregate in cementitious mortars

Aziz Hasan Mahmood · Sumaiya Afroz · Alireza Kashani  · Taehwan Kim · Stephen J. Foster

Received: 28 December 2021 / Accepted: 3 June 2022 / Published online: 29 June 2022  
© The Author(s) 2022

**Abstract** With the potential for a decline in fly ash (FA) production over time, due to the phasing down of coal fired power plants, alternative supplementary cementitious materials need to be identified. The efficiency of pulverised glass powder (PGP) was studied for its reactivity and its capacity for inhibiting alkali-silica reaction (ASR) that results from utilisation of recycled glass as a fine aggregate (sand) replacement. Characterisations of pastes containing PGP reveal that PGP may possess latent hydraulic properties, resulting in a more than 75% strength activity index, together with better strength gain than FA-blended pastes. PGP also offered increased heat of hydration compared to FA, from a combination of the dilution effect, filler effect and early-age reactions of PGP. A comparable efficiency of PGP and FA in ASR expansion mitigation was confirmed with mortar bar expansions of less than 0.10% at cement replacement levels of at least 10%. Both PGP and FA provided alkali dilution and reduced the mass transport in hydrated cement paste from the refinement of larger pores to below 60 nm. The FA mix consumed calcium hydroxide and, thus, performed marginally better than the PGP mix in mitigating ASR. This pozzolanic

reactivity is not evident for PGP, whereas in the literature glass powders are often regarded as pozzolanic. Microscopic images confirm that PGP and FA significantly limit the occurrence of ASR gels without altering its composition. It was concluded that PGP is a comparable ASR inhibitor to FA, despite the underlying differences in their mechanisms. The result of this research support the utilisation of recycled glass both as an aggregate, and as an ASR-inhibiting SCM in cementitious systems.

**Keywords** Pulverised glass powder · Fly ash · Glass fine aggregate · Alkali-silica reaction

## 1 Introduction

Around 56% of post-consumer glass, particularly from packaging, is recycled in Australia (about 0.62 million tons), leaving the rest to be stockpiled or disposed of in landfill [1]. The stringent benchmark for glass products often limits the capacity for waste glass to be recycled to its original form, especially because of contamination with sugars, paper, tags, and blending of different coloured glasses in co-mingled recycling practice. A technical solution towards sustainable utilisation of recycled glass can be adaption as a component used in the manufacture of concrete. The current global aggregate consumption in concrete stands at 17.5 billion tons and the replacement of

---

A. H. Mahmood · S. Afroz · A. Kashani (✉) · T. Kim · S. J. Foster

Centre for Infrastructure Engineering and Safety, School of Civil and Environmental Engineering, The University of New South Wales, Sydney, NSW 2052, Australia  
e-mail: ali.kashani@unsw.edu.au



natural aggregates with recycled glass can offer an effective pathway for value-added utilisation, not just in traditional concrete-making, but also in alkali-activated and foam concrete [2–4]. The use of glass fine aggregate (GFA) in concrete can be dated back to the 1950s but the durability of the manufactured concrete was questioned upon detection of the alkali-silica reactivity of glass [5].

Alkali-silica reaction (ASR) is a complex chemical reaction between reactive aggregates (e.g., recycled glass), hydroxyl and alkali ions in concrete pore solution. Continuing research in understanding the mechanism behind ASR identifies three criteria [6, 7] that need to be aligned for the reaction: (i) high alkali content in concrete pore solution; (ii) presence of moisture; and (iii) availability of reactive silica. Calcium ions present in the pore solution also play an essential role in the initial ASR gel formation and its subsequent expansion [8–11]. Recycled glass is mostly composed of an amorphous phase and, thus, can dissolve in the highly alkaline pore solution of the cementitious composite. The dissolved silica undergoes a series of chemical changes, including hydration, to form soluble silicate species (mainly  $\text{H}_3\text{SiO}_4^-$  and  $\text{H}_2\text{SiO}_4^{2-}$ ) that associate with available  $\text{K}^+$ ,  $\text{Na}^+$ , and  $\text{Ca}^{2+}$  ions in the pore solution. The resultant chemical reaction is the formation of insoluble poly-metal silicates. Flocculation and condensation of these silicates form hydrophilic ASR gels, which swell from water absorption and result in expansion. The expansive nature of ASR gel formed in concrete can initiate internal cracks from the pressure exerted, threatening a concrete's durability. Details about the ASR mechanism are further explained in [7, 10, 12–16].

ASR expansions in concrete can be limited with addition of mineral additives as supplementary cementitious materials (SCMs) [17–19]. In this context, the role of fly ash (FA) has been investigated in detail [19–21]; several mechanisms contribute to a reduced ASR expansion, such as alkali binding [22, 23], alkali dilution [24, 25], Portlandite consumption [26, 27], limited mass transport [28], and aluminium discharge from FA to control the dissolution of reactive aggregates [21]. However, the continually increasing demand for FA in the construction industry may not be met in the future due to declining production in coal-fired power generation, with a shift towards alternate sources of energy production [29].

Thus, exploration is needed to find other sustainable sources of SCMs for ASR mitigation in concrete.

Pulverised glass powder (PGP) has recently gained attention as a potential alternative to FA. The argument for PGP as an ASR suppressor relies on its pozzolanic reactivity for ASR mitigation [30–33]. In addition, PGP limits the dissolution of amorphous silica from reactive aggregates by discharging aluminium in the pore solution [34] and reducing the alkalinity in the vicinity of the reactive aggregates [35]. While the “pessimum” level of fineness of the reactive aggregates (e.g., glass aggregate) causes the maximum expansion [36, 37], a reduced expansion is observed when glass is ground to a smaller size of less than 0.30 mm [38]. As such, PGP can inhibit the ASR expansion of glass fine aggregate (GFA) in concrete [31, 32, 39]. However, the ASR suppression from the use of PGP cannot be universally attributed to its pozzolanic reactivity despite its recent standardisation as a pozzolan for use in concrete in ASTM C1866M–20 [40]. For instance, Dyer and Dhir [41] observed no evidence of Portlandite consumption while replacing 40% cement with PGP and confirmed no enhancement in the degree of reaction. In a separate study, Ramadan et al. [42] reported a weak pozzolanic reactivity of a glass powder even when ground to a 20  $\mu\text{m}$  median particle size; Jang et al. [43] and Aliabdo et al. [44] reported a latent hydraulic property of powdered glass. This deviation from the expected outcome emphasises the inherent differences in the quality of glass that can dictate its pozzolanic reactivity due to contrasting chemical composition, fineness, and the quantity of glassy phase. Despite soda-lime glass (Type GS) and E glass (Type GE) being standardised as pozzolans [40], the reactivity of mingled glasses, the most common form of recycled glass, needs further assessment to complement the current understanding of the reactivity of glass.

This research is aimed at providing evidence on the efficiency of PGP sourced from mixed coloured recycled glass to inhibit the ASR expansion derived from the use of mixed glass as fine aggregate. The study focuses on understanding the underlying mechanism of ASR mitigation by using recycled glass powder and its differences compared to fly ash including its pozzolanic reactivity. The results can assist in strategising safe use of glass in concrete both in aggregate and binder form and promote global acceptance in country-specific standardisations for



locally sourced recycled glass. To this extent, the reactivity of PGP as a mineral additive to cement paste is assessed by different techniques, including (i) strength activity index (SAI), (ii) the heat evolution during the hydration, (iii) the consumption of Portlandite, and (iv) modifications in the pore structure. An accompanying set of specimens with low-calcium FA is also studied to provide a systematic comparison against PGP. Subsequently, the efficiency of PGP to mitigate ASR expansion of recycled glass fine aggregate (GFA) is explored using the accelerated test method outlined in ASTM C1567 [45].

## 2 Materials and experimental methods

### 2.1 Binders and SCMs

An Australian General Purpose (GP) cement conforming to AS 3972 [46] was used in this study. Low-calcium FA conforming to AS 3582.1 [47] and PGP were sourced locally, and their reactivity was assessed through a series of analytical techniques to investigate the expansion mitigation induced by ASR. The chemical composition of the cement, FA, and PGP was determined by wavelength-dispersive X-ray fluorescence (WDXRF) technique in a PANalytical Axios Advanced WDXRF spectrometer, and the results are summarised in Table 1. To conduct the WDXRF, fused glass bead samples were prepared from each material used in this study. Meanwhile, the loss on ignition (LOI) was measured on sub-samples at the same temperature as the beads. The LOI of the cement may have originated from the limestone addition of up to 7.5% [46] in the commercially available Australian GP cement. The GP cement used in this study contains 5.9% calcite, which was determined by thermogravimetric analysis (TGA). The specific gravity of the cement, FA, and PGP were determined as 3.20, 2.66, and 2.80, respectively using ASTM C188 [48] procedure.

The particle size distribution (PSD) of the binders was determined with laser diffraction technique in a Malvern Mastersizer 2000 instrument. The  $D_{10}$ ,  $D_{50}$ ,  $D_{90}$  values of the binders are presented in Table 2 determined from the PSDs illustrated in Fig. 1. The PGP obtained from the supplier (coarse PGP) was significantly coarser than the cement and FA used in this study with a median diameter  $D_{50}$  of about 80

**Table 1** Chemical composition, LOI, and specific gravity of cement, FA, and PGP

Chemical oxide	Chemical composition by mass (%)		
	GP cement	FA	PGP
SiO <sub>2</sub>	19.15	63.61	71.59
Al <sub>2</sub> O <sub>3</sub>	4.76	25.60	1.37
CaO	64.18	1.87	10.92
Na <sub>2</sub> O	0.26	0.55	12.67
MgO	1.28	0.56	0.48
Fe <sub>2</sub> O <sub>3</sub>	3.04	3.17	0.45
Mn <sub>3</sub> O <sub>4</sub>	0.05	0.04	0.09
P <sub>2</sub> O <sub>5</sub>	0.09	0.27	0.02
SO <sub>3</sub>	2.44	0.07	0.02
K <sub>2</sub> O	0.43	1.28	0.29
TiO <sub>2</sub>	0.22	0.95	0.05
BaO	0.01	0.02	0.02
ZnO	0.05	–	0.07
Cr <sub>2</sub> O <sub>3</sub>	0.01	–	0.05
CuO	0.01	–	0.01
Loss on ignition (LOI)	3.57	1.73	0.78
Specific gravity	3.20	2.66	2.80

**Table 2** Percentile values as determined from the particle size distribution of cement, FA, and PGP

Material	$D_{10}$ (μm)	$D_{50}$ (μm)	$D_{90}$ (μm)
GP Cement	2.7	17.1	41.9
FA	2.3	16.5	51.3
Coarse PGP (as received)	29.9	80.9	162.8
Fine PGP (after milling)	4.1	19.3	52.1

microns, over four times the size of cement and FA. To maintain a similar PSD, the coarse PGP was milled in a Fritsch Pulverisette 6 planetary mono mill resulting in fine PGP with a median particle size  $D_{50}$  of 19.3 microns.

The mineralogical characterisation of the binders was achieved using X-ray diffraction (XRD) analysis in a Philips X'pert MPD (multi-purpose X-ray diffractometer) and data were qualitatively processed with High Score Plus software. The phases identified are presented in Fig. 2. The raw GP cement shows several minerals including Alite ( $C_3S$ ), Belite ( $C_2S$ ), Tricalcium aluminate ( $C_3A$ ), and Ferrite ( $C_4AF$ ) with traces of gypsum ( $CaSO_4 \cdot 2H_2O$ ). The unreacted FA

**Fig. 1** The particle size distribution of binders: **a** percentage passing; **b** differential

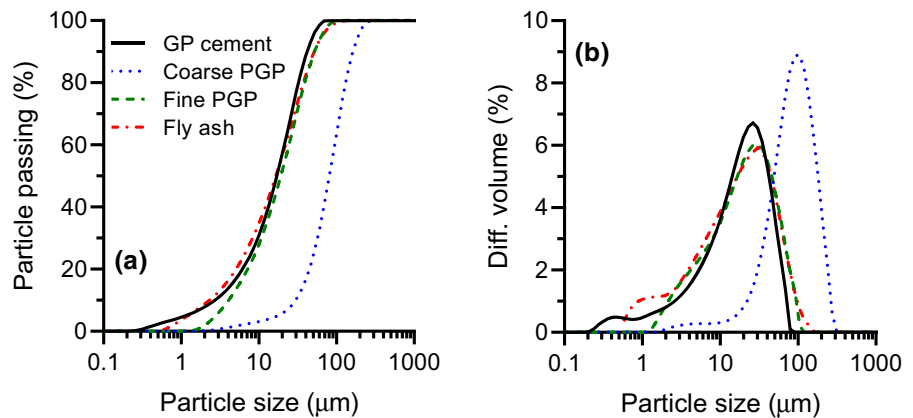
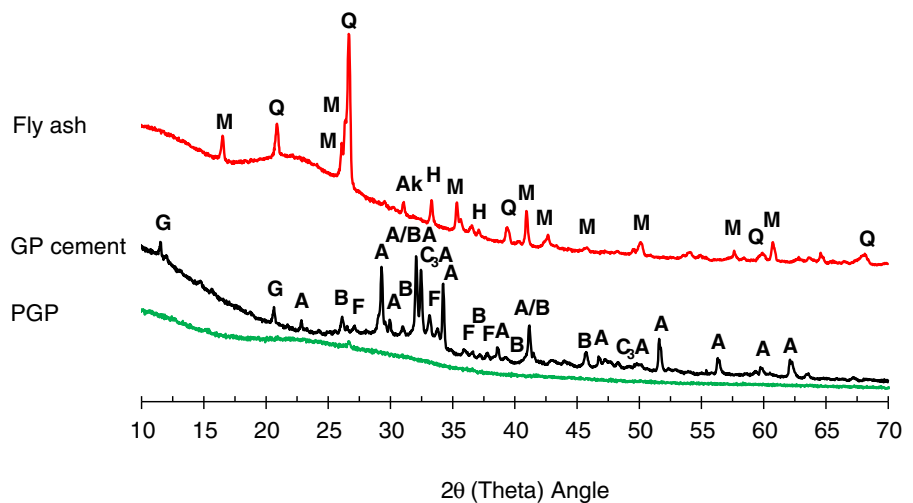


**Fig. 2** XRD patterns of cement, FA, and PGP [*M*—Mullite ( $\text{Al}_6\text{Si}_2\text{O}_{13}$ ); *Q*—Quartz ( $\text{SiO}_2$ ); *Ak*—Akermanite ( $\text{Ca}_2\text{Mg}_{0.54}\text{Al}_{0.92}\text{Si}_{1.54}\text{O}_7$ ); *H*—Hematite ( $\text{Fe}_2\text{O}_3$ ), *G*—Gypsum ( $\text{CaSO}_4 \cdot 2\text{H}_2\text{O}$ ); *A*—Alite  $\text{C}_3\text{S}$  ( $3\text{CaO} \cdot \text{SiO}_2$ ); *B*—Belite  $\text{C}_2\text{S}$  ( $2\text{CaO} \cdot \text{SiO}_2$ ); *C}\_3\text{A}*—Tricalcium Aluminate  $\text{C}_3\text{A}$  ( $3\text{CaO} \cdot \text{Al}_2\text{O}_3$ ); *F*—Ferrite  $\text{C}_4\text{AF}$  ( $4\text{CaO} \cdot \text{Al}_2\text{O}_3 \cdot \text{Fe}_2\text{O}_3$ )



shows crystalline phases of Mullite, Quartz, Hematite, and small but detectable traces of Akermanite together with amorphous phases detected in the wide diffraction bump in the 17–30° ( $2\theta$ ) range [49]. In contrast, PGP exclusively shows a hump centred at around 25° ( $2\theta$ ) with no recognisable crystalline peak in its XRD pattern, which confirms the strong amorphous nature of PGP. The SEM micrographs of raw GP cement, FA, and coarse PGP are shown in Fig. 3 outlining the differences in their morphology.

## 2.2 Aggregates

Double-washed natural river sand and crushed glass fine aggregate (GFA) were used as fine aggregates in the preparation of mortar samples to evaluate the ASR potential of GFA. The river sand was sourced from the Ardmore Park Quarry in NSW while the GFA was

supplied by a glass recycling facility in Tuncurry, NSW. To minimise contamination (organic residue, paper tags, sugar, etc.), the GFA was washed and pre-treated at elevated temperatures prior to supply. The absence of sugar in the glass fine aggregate (GFA) was confirmed by undertaking the procedure described in AS 1141.35 [50]. The water absorption of the river sand and GFA were measured at 3.5% and 0.1%, respectively, following the procedures described in AS 1141.5 [51]. The GFA water absorption is significantly lower than natural river sand due to its non-porous texture. The specific gravity of river sand and GFA are 2.62 and 2.32, respectively.

## 2.3 Experimental methods

A list of all the tests undertaken in this study is outlined in Table 3 with the mixture proportion

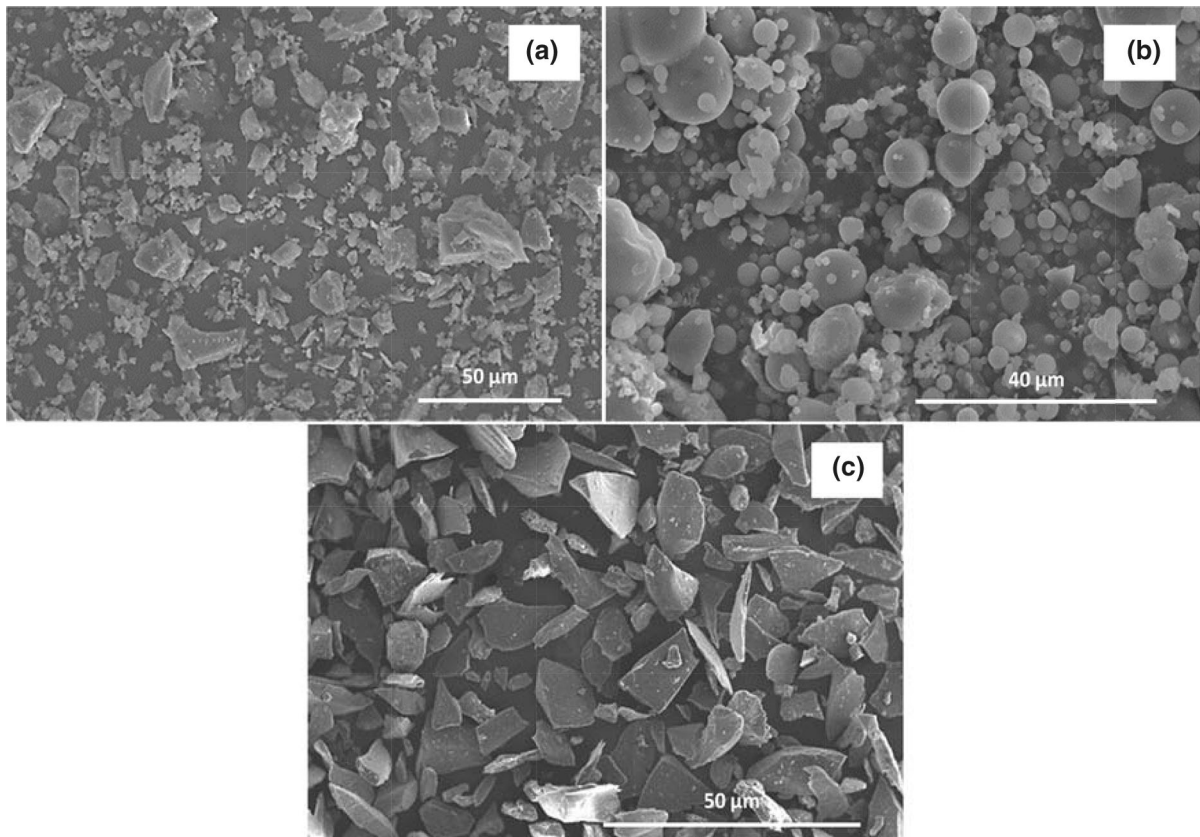


**Fig. 3** SEM micrographs of raw binders: **a** GP cement; **b** FA; **(c)** Coarse PGP

parameters adopted for each test. The individual test method procedure is detailed in the subsequent sections.

### 2.3.1 Strength activity index (SAI) test

To determine whether, or not, PGP results in an acceptable level of strength development when used as an SCM, a strength activity index (SAI) test was undertaken as per ASTM C311 [52] procedure. The strength development of the mixes with SCMs summarised in Table 3 was evaluated against a cement-based control mix while 20% of the cement was replaced by FA and PGP (both coarse and fine). Six mortar cubes were prepared for each control and test mixture and tested under compression at the age of 7 days and 28 days.

### 2.3.2 Heat evolution of pastes

The effect of FA and PGP on the heat of hydration of cement was investigated by monitoring the heat evolution in a TAM Air isothermal calorimeter (TA instruments); the isothermal condition was maintained at 23 °C. For each test, 6 g of paste sample was prepared by manual-mixing in a 20 ml glass ampoule, quickly followed by loading the specimen into the calorimeter. Each test sample was accompanied by an inert reference sample (quartz sand) with the same heat capacity as the 6 g test sample. The heat evolved in the first 72 h of hydration was measured for determining the heat flow and the cumulative heat of hydration. Each test was repeated to gather at least two sets with similar results.

### 2.3.3 Thermogravimetry analysis (TGA)

Thermal analyses of the cement pastes with and without SCMs (20% replacement) were undertaken;

**Table 3** Summary of the experimental program with mixture proportions of paste and mortar samples

Sample description	Mix ID	Binder (%)			Aggregate (%)		W/B ratio	Test description
		Cement	FA	PGP	River sand	GFA		
Mortar	Control	100	–	–	100	–	0.48	SAI
	PGP (Coarse)	80	–	20	100	–	0.48	SAI
	PGP (Fine)	80	–	20	100	–	0.48	SAI
	Fly ash	80	20	–	100	–	0.48	SAI
Paste	Control	100	–	–	–	–	0.48	TGA, NAD, HE
	10FA	90	10	–	–	–	0.48	HE
	20FA	80	20	–	–	–	0.48	TGA, NAD, HE
	10PGP	90	–	10	–	–	0.48	HE
	20PGP	80	–	20	–	–	0.48	TGA, NAD, HE
Mortar (AMBT test series)	100GP-100GFA	100	–	–	–	100	0.47	AMBT
	100GP-40GFA	100	–	–	60	40	0.47	AMBT, SEM-EDS
	100GP-20GFA	100	–	–	80	20	0.47	AMBT
Mortar (AMBT mitigation series)	10FA-40GFA	90	10	–	60	40	0.47	AMBT, SEM-EDS
	10FA-20GFA	90	10	–	80	20	0.47	AMBT
	20FA-40GFA	80	20	–	60	40	0.47	AMBT
	20FA-20GFA	80	20	–	80	20	0.47	AMBT
	10PGP-40GFA	90	–	10	60	40	0.47	AMBT, SEM-EDS
	10PGP-20GFA	90	–	10	80	20	0.47	AMBT
	20PGP-40GFA	80	–	20	60	40	0.47	AMBT
	20PGP-20GFA	80	–	20	80	20	0.47	AMBT

SAI Strength activity index, TGA Phase analysis by thermalgravimetric analysis, NAD Microstructure by nitrogen adsorption and desorption isotherms, HE Heat evolution by isothermal calorimetry, AMBT Accelerated mortar bar test, SEM-EDS Scanning electron microscopy—Energy dispersive spectroscopy

the paste mixes tested are outlined in Table 3. To study temporal changes in microstructural properties, the hydration of the specimens was stopped at selected times (7, 14, 28, and 56 days), with the paste samples cast in plastic containers and stored at 23 °C until the day of testing. On each test day, fragments from the core of the sample were collected and milled in a Fritsch Pulverisette 6 planetary mono mill equipped with a tungsten carbide grinding bowl and bearing balls.

The solvent exchange method suggested by RILEM TC-238 SCM [53] recommendations, with two modifications, was used to end hydration in the test specimen. The modifications were: (i) the duration of solvent exposure was extended from 15 to 60 min; and (ii) drying was extended from 8 to 30 min to confirm absolute hydration stoppage. The modifications were undertaken to ensure sufficient exchange to stop hydration without damaging the microstructure based

on the works of Zhang and Scherer [54]. The test specimens were immersed in isopropanol (at a dose of 3 g per 100 mL) and agitated with a magnetic stirrer (60 min for 3 g of test specimen). The dispersed test specimen was then vacuum filtered through a membrane filter. The residue on the filter was cleaned once with isopropanol and twice with diethyl ether on the filter paper and then dried on the filter paper, at 40 °C in a ventilated oven for 30 min. Finally, specimens were placed in plastic vials and stored in an N<sub>2</sub> atmosphere glove box. Any remaining air within the plastic vial was released and replaced with N<sub>2</sub> gas.

The thermogravimetric analyses (TGA) were conducted in a Q600 SDT from TA instruments. Approximately 30 mg of the test specimen was placed in an alumina crucible and loaded into the instrument. The specimens were left at an isothermal condition for 10 min and the subsequent thermal analysis was performed under a 50 mL/min N<sub>2</sub> gas flow



atmosphere. The temperature ranged from 23 to 1000 °C at a rate of 10 °C/min. The TGA curves of the paste samples were interpreted following the tangential method suggested in the previous literature [55] to quantify the CH content at the ages of 7, 14, 28, and 56 days.

#### 2.3.4 Pore structure measurement ( $N_2$ adsorption–desorption isotherm)

To register the transition of structures of gel and median capillary pores from young to mature ages, nitrogen adsorption–desorption isotherms (NADs) were determined using a NOVAtouch LX gas sorption analyser. The paste samples prepared for TGA were used to determine NADs for 7, 14, 28, and 56 days. For measuring the NADs, the samples were degassed for 16 h at 40 °C under vacuum conditions to remove any physically adsorbed gases. The degassing was undertaken in a vacuum instead of gas flow to remove water from the fine pores for pore structure determination as suggested by Scrivener et al. [56]. The adsorption branches of isotherms were analysed employing the Barrett, Joyner and Halenda (BJH) method [57] because the pore size distribution is the main interest of this study. The desorption branch cannot provide a reliable pore size distribution for a complex pore structure (such as cementitious materials) where network effects (pore-blocking and cavitation) significantly affect the desorption isotherm [58, 59]. This method assumes pores in hydrated cement products to be cylindrical and has been utilised to investigate pore sizes up to 60 nm in radius [60–62]. Due to the assumption, the BJH method only provides limited information but is still reasonably effective in the qualitative analysis of cementitious materials [52, 57, 58], at least for comparative analysis.

#### 2.3.5 Accelerated ASR test

The potential for expansion due to ASR of GFA was measured using standard mortar bar testing following ASTM C1260 [63] and its Australian Standard counterpart AS 1141.60.1 [64]; the test procedure is known as the accelerated mortar bar test (AMBT). The potential of PGP in mitigating the expansion induced by ASR of GFA was investigated following ASTM C1567 [45] guidelines and compared to that of FA.

Two series of experiments were undertaken: (i) the test series utilised GFA in different proportions in a 100% cement binder and (ii) the mitigative series incorporated FA and PGP as SCMs. Details of these mixes are summarised in Table 3. In the test series, cement mortars with varying fine aggregate replacement ratios of 20%, 40% and 100% (by mass) were investigated to classify the aggregates based on expansions. The mitigation series replaced GP cement with FA and PGP at 10% and 20% keeping the GFA proportions in the mixes to be 20% and 40%. Other mixture parameters, mixing procedure, sample preparation, conditioning, and data collection were maintained according to the standards. All specimens were exposed to 1 mol/L NaOH solution at 80 °C. At the end of 14 days (ASTM C1260 [18]) and 21 days (AS 1141.60.1 [11]) of exposure, each aggregate portion was classified according to the criteria outlined in Table 4 based on the expansions recorded. For the mitigation series in Table 3, ASTM C1567 [19] guidelines were followed. In the mitigation series, FA and PGP replaced cement, and mortar bar expansions of less than 0.10% after 14 days of zero reading were defined as acceptable expansions with the aggregate being classified as “innocuous”. Three standard prism specimens were used for all AMBT tests.

#### 2.3.6 Microstructural analysis of mortars after AMBT test

The morphology of ASR gel in the AMBT test samples after the test duration was observed employing a Hitachi 3400 scanning electron microscope with energy dispersive spectroscopy (SEM–EDS). For this purpose, SEM samples of about 2–3 mm thickness were saw-cut with a slow rotating diamond saw. The thin slices were then embedded in epoxy resin and the test surface was ground on emery papers before polishing with diamond paste with progressively smaller grit (6 µm, 3 µm and 1 µm diamond polishing paste) to ensure ideal image quality. An Emitech K575x Pt sputter coater was employed to coat the sample surface with 20 nm Pt sputters under vacuum conditions. The coating ensured that there is no accumulation of electrons (charging) on the non-conductive specimen surface and a clear image is obtained. The microscope was operated under backscattered electron (BSE) mode at an accelerating current of 30 amps and 20 kV voltage, ensuring



**Table 4** Comparison between ASR reactivity thresholds in ASTM C1260 [63] and AS 1141.60.1 [64]

ASTM C1260		AS 1141.60.1		
Interpretation	14 days expansion (%)	Classification	10 days expansion (%)	21 days expansion (%)
Innocuous	< 0.10	Non-reactive	–	< 0.10*
Uncertain	0.10–0.20	Slowly reactive	< 0.10*	0.10*–0.30
Potentially deleterious	> 0.20	Reactive	≥ 0.10*	–
		Reactive	–	≥ 0.30

\*The value for natural fine aggregates is 0.15%

1300 ± 300 counts per second. The backscattered EDS was corrected using a peak to background (P/B) ZAF correction to obtain the semi-quantitative elemental composition.

### 3 Results and discussions

#### 3.1 Reactivity of FA and PGP

To evaluate the reactivity of coarse and fine PGP and to provide a comparison against low-calcium FA, their strength activity indices (SAIs) were determined as illustrated in Fig. 4, together with respective strength gains in 7 days and 28 days. As expected, cement

substitution with 20% PGP and FA resulted in comparatively lower strengths than the control in both seven and 28 days. The degree of strength reduction was, however, dependent on the SCM used; coarse PGP reached the lowest level of strength, followed by FA and fine PGP, respectively. Although derived from the same source, the mortar with the fine PGP reached 52% higher compressive strength than the mortar with coarse PGP in 28 days, highlighting the influence of the fineness of PGP on strength gain. In addition, the fine PGP (that had similar PSD to that of FA, as shown in Fig. 1) achieved more than 15% higher compressive strength than FA mortars. It is hypothesised that this variation in strength is related to the difference in their chemical compositions. The fine PGP achieved the

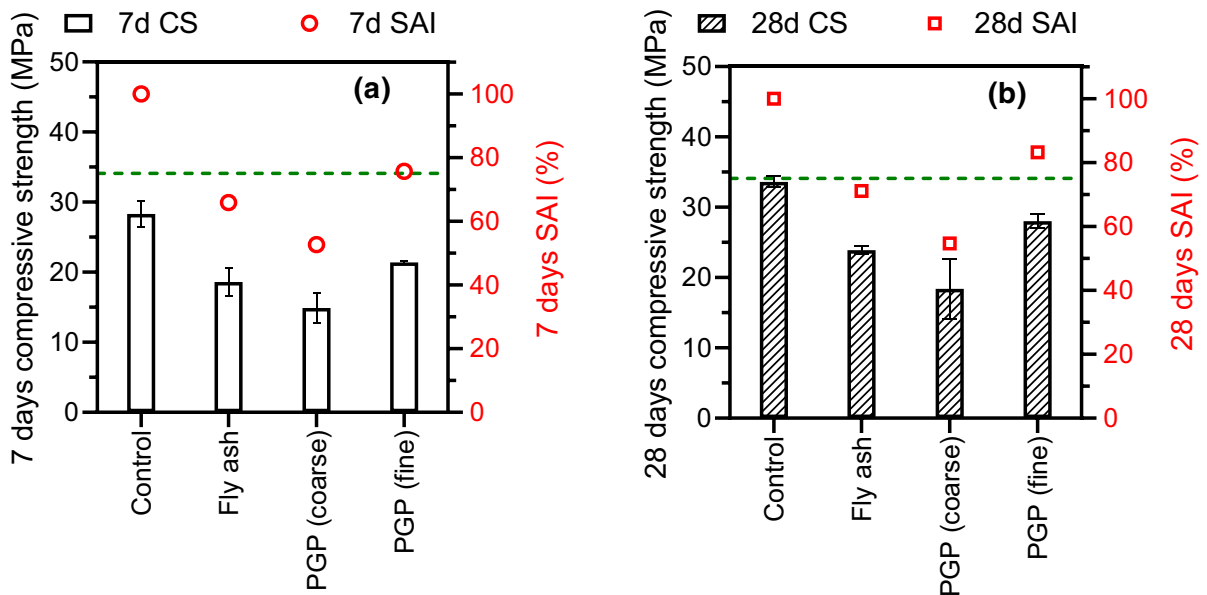


**Fig. 4** Compressive strength and strength activity index (SAI) of mortars with no SCM (control), and with SCM—20% FA, coarse PGP, and fine PGP: **a** 7 days; **b** 28 days. The dotted lines

refer to 75% SAI recommended in ASTM C618-19 to determine potential pozzolanic reactivity





highest SAI followed by FA and coarse PGP, respectively. More importantly, the SAI of the coarse PGP and FA failed to reach 75% of the control while only the fine PGP reached the mark in both seven and 28 days. Therefore, the fine PGP conforms to the requirements set by ASTM C618-19 [65] to be regarded as a pozzolan (particularly Class N). It should be noted that the FA used in this study closely failed to reach the Class F criteria in ASTM C618-19 due to the SAI index being less than 75%. However, this FA conforms to AS 3582.1 [47] and is a widely used commercial product in Australia. The reactivity of the fine PGP can derive from its highly amorphous structure, relatively high contents of  $\text{Na}_2\text{O}$  and  $\text{CaO}$  (more than 10%, as seen in Table 1), and the significantly low LOI in contrast to cement and FA. The relatively high alkali and  $\text{CaO}$  content may contribute to enhanced cement hydration [66], leading to better strength development, particularly in the first 28 days of hydration [67]. An inverse relationship between LOI of SCMs and compressive strength was also reported in the previous studies [68, 69] and thus may corroborate the higher strength gain of fine PGP. However, the nature of this reactivity of PGP was assessed to be latent hydraulic in nature, as discussed further in Sects. 3.2 and 3.3 of this paper.

The current classification methods for pozzolans, particularly ASTM C618-19 [65] is somewhat subject to interpretation, as the factors outlined in the standard to classify pozzolans such as, LOI, chemical oxide composition, and fineness, cover a broad range and materials, and within the range different performances may be observed. In addition, factors such as the quantity of amorphous phase and ability to consume CH are not reflected. These parameters can change even for certain well-recognised pozzolans (e.g., FA), depending on their source, and this variability is unavoidable. The pozzolanic property of the fine PGP, although conforms to the standardised definition and is in line with findings in the literature [34, 70, 71], cannot be taken as absolute without undertaking further analytical assessments. The SAI on its own may not provide a decisive outcome to characterise PGP as pozzolan because some anomaly may exist between the index and its true performance as a pozzolan [72]. As such, further technical evidence is gathered in this research to assess fine PGP's performance as an SCM. Nevertheless, the SAI test provided a comparative outcome, especially in demonstrating

the higher reactivity of PGP when ground to a finer median size of 19.3  $\mu\text{m}$ .

### 3.2 Heat evolution of pastes

The effects of cement substitution with FA and PGP on the rate of heat evolution (normalised to unit mass of binder and unit mass of cement) were investigated using an isothermal calorimeter and data is presented in Fig. 5. The typical stages of cement hydration [73] are observed in both heat flow curves in Fig. 5a, c. An initial peak of high magnitude occurs within approximately 30 min of hydration, which corresponds to the binder wetting and dissolution, followed by a short induction period. The end of the induction period marks the onset of the first acceleration period that reaches the peak at around 9–10 h. At this stage, two distinct peaks can be identified for all paste mixes. The first peak corresponded to the accelerating growth of cement hydration products (C–S–H), mainly through the hydration of alite ( $\text{C}_3\text{S}$ ). The second peak (also known as the sulphate depletion peak [74]) featured further formation of ettringite from hydration of the aluminate phases ( $\text{C}_3\text{A}$  and  $\text{C}_4\text{AF}$ ) [75]. The gypsum identified in Fig. 2 controls the rate of the aluminate phase hydration to avoid flash set and loss of workability. Following the sulphate depletion peak, the heat flow was decelerated, indicating the decreasing hydration reaction rate [76]. The heat flow curve flattened beyond the deceleration and hydration continued in a steady-state phase as marked by the growing cumulative heat curves in Fig. 5b, d.

Normalising the heat of hydration to the total mass of binder and cement provides important information. The reduced heat flow and cumulative heat of Fig. 5a, b could mainly be the result of the dilution effect of both FA and PGP; the dilution is more prominent at a higher replacement level of 20%. However, at the same replacement level of PGP and FA, greater heat was generated in the PGP pastes than that of FA pastes, indicating the relatively superior reactivity of PGP. This higher cumulative heat of PGP pastes may corroborate the higher strength achieved in the SAI tests illustrated in Fig. 4. When heat flow is normalised per gram of cement (Fig. 5c), an increase in the heat flow is evident with the inclusion of SCMs. Both FA and PGP acted as fillers between cement grains, providing extra space and nucleation sites for the hydration products at the same water to binder

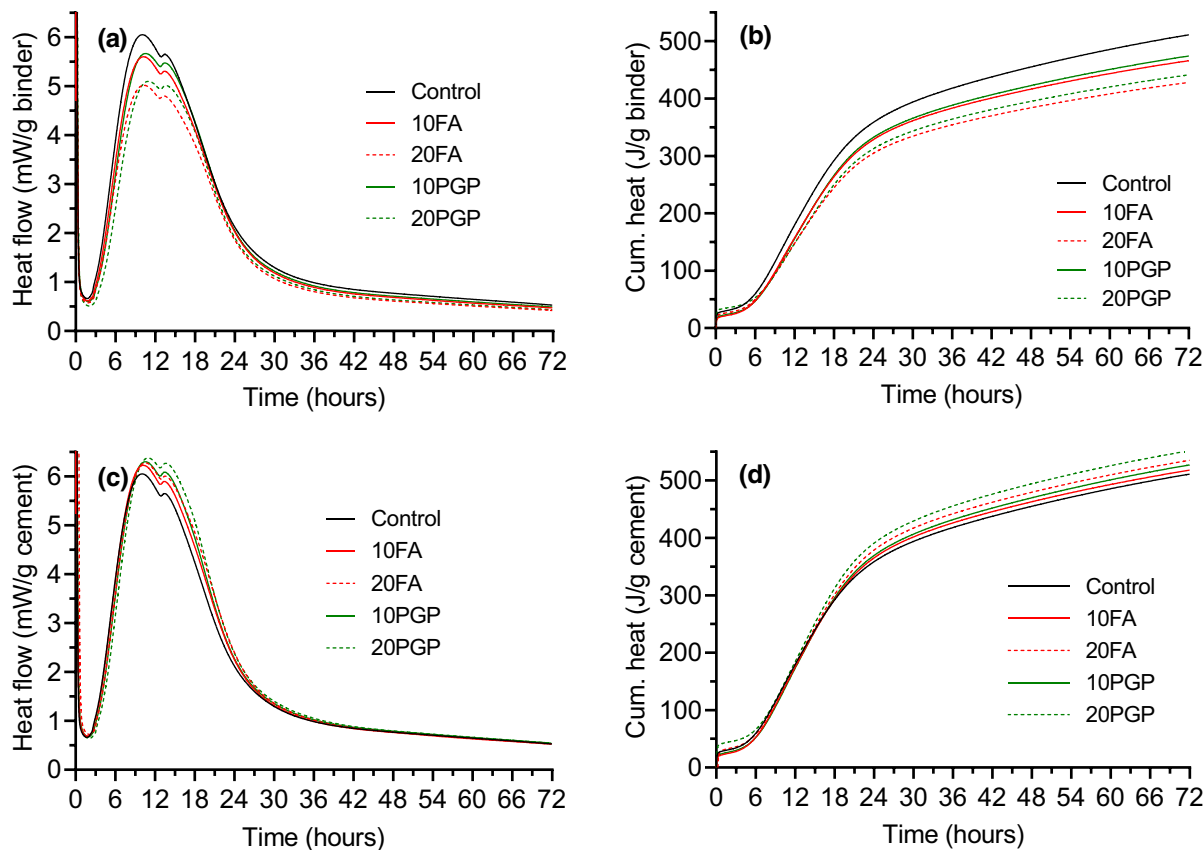


**Fig. 5** Isothermal calorimetry curves for cement paste and pastes with 10% and 20% SCM: **a** heat flow per g of binder; **b** cumulative heat per g of binder; **c** heat flow per g of cement; and **d** cumulative heat per g of cement

(total solids) ratio [28, 77]. This filler effect was also reflected in the cumulative heat curves presented in Fig. 5d. With the addition of FA and PGP, the cumulative heat released per unit mass of cement increased; the rate is higher for a higher degree of substitution. Interestingly, PGP offers a higher heat flow than FA at the same replacement levels. Considering Class F fly ash are inert in the first 24 h of hydration, this increased heat release using PGP may indicate an early-age reaction potential of PGP. The previous studies [43, 44] also showed some extent of hydraulic property of powdered glass due to its CaO content.

It is noteworthy that the nature of the heat flow curves in Fig. 5a, c did not alter with the addition of FA and PGP—the slope of the acceleration curve remains almost identical. However, critical features were still noticeable with the time of occurrence of the acceleration and the sulphate depletion peaks. With the addition of SMCs, the acceleration peak was

slightly delayed by approximately 20 min and 30 min for 10% and 20% FA, and 30 min and 50 min for 10% and 20% PGP addition. This delay suggests that both FA and PGP retards cement hydration to some extent with a relatively longer induction period. The literature reports that fly ash causes the delay from two competing phenomena—increase in the nucleation sites and retardation due to the adsorption of  $\text{Ca}^{2+}$  that would otherwise take part in CH formation [78, 79]. A similar mechanism may or may not explain the delay for PGP inclusion. However, by providing extra nucleation sites for cement hydration (as reflected in Fig. 5c), both SCMs counterbalance the retardation and thus, the delay in the formation of acceleration peak is marginal.

### 3.3 Thermogravimetric analysis (TGA)

The CH contents obtained from control, 20PGP, and 20FA using TGA are compared in Fig. 6 for up to

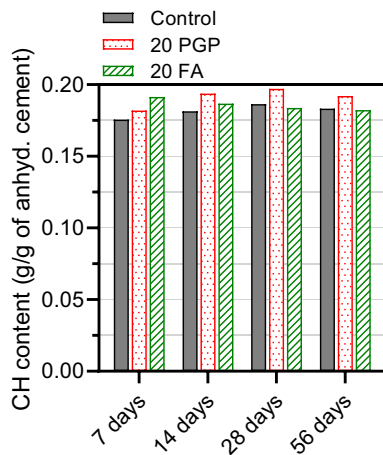


**Fig. 6** Calcium hydroxide contents derived from TGA curves using the modified interpretation method [55]

56 days of hydration. A gradual increase in the CH content for the control cement paste was observed up to 28 days, as expected, indicating continuing hydration of the cement. The CH content in the first four weeks of hydration could be linked to the hydration of alite ( $C_3S$ ). However, following 28 days, a small drop in CH (0.0032 g/g of anhydrous cement) was observed in the cement paste. Such a small change may be the experimental error caused by the detection limit of the data. The 5.9% calcite in the GP cement used in this study may form carboaluminates at a later age [80], triggering a slight drop in CH content in control and 20PGP between 28 and 56 days. Weerdt et al. [81] observed a similar drop in CH content in cement paste with 5% limestone and attributed the drop to secondary effect of carboaluminate formation or simply dilution effect.

On day seven, the CH content per gram of anhydrous cement in the pastes with 20% of FA and PGP was slightly higher than that obtained from the control. This seems to be due to the filler effect of FA and PGP as also identified in heat flow curves which increase the hydration degree of the cement particles.

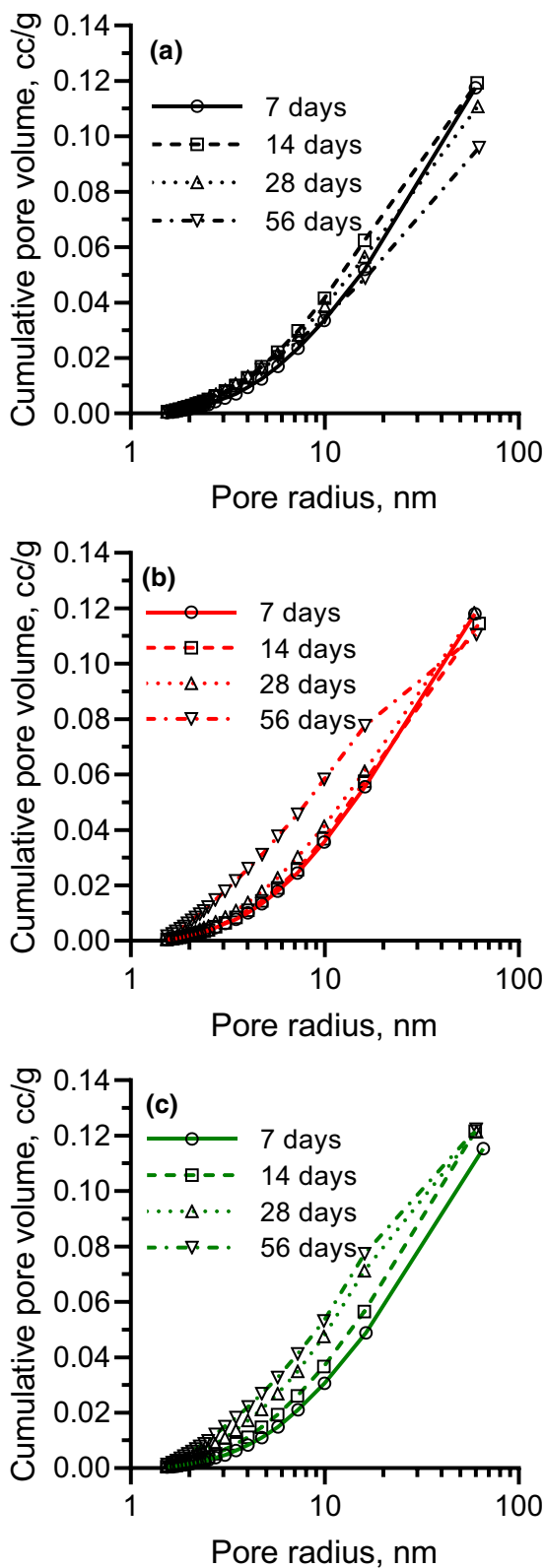
As the pastes mature to 56 days, the consumption of CH in the FA paste was evident with a steady decline in the CH content over time. The declining trend suggested the FA's continuing pozzolanic reaction in consuming CH to produce secondary C–S–H in the system [81]. Attention can be drawn to the SAI of FA in Fig. 4—in 28 days, the FA specimens reached 71% strength of the control as opposed to 66% in 7 days.

The TGA suggested that the pozzolanic reactivity of FA caused this improved strength at a later age. However, a contrasting observation was made for the paste with PGP. There is no clear evidence of CH consumption in Fig. 6 for 20% PGP replacement. On day 56, the relatively lower CH in the PGP paste may be attributed to the reaction of limestone of the GP cement to produce hemicarbonates [81], and may not originate from CH consumption by PGP. The CH content of the PGP sample was still greater than the control at 56 days, indicating enhanced hydration of the cement from the filler effect, a mechanism also corroborated by the calorimetric analyses.

Since the thermal analysis could not confirm the pozzolanic reactivity of PGP, the question remains as to the reasons for the significantly enhanced compressive strength achieved with PGP in the SAI test. The PGP used in this study may possess a latent hydraulic property that would explain the SAI achieved (more than 75%) in both 7 and 28 days of hydration. Suraneni et al. [82] observed a similar increasing trend of CH over time when using solid waste incineration FA with relatively higher CaO content. Another hypothesis is that glass constituents, instead of Ca from cement, get incorporated in forming of the CSH gels during hydration, allowing more CH to be formed [41]. The PGP of this study, with about 11% CaO, may have prompted a similar mechanism; i.e., latent hydraulic reactivity while undergoing possible hydration of PGP.

### 3.4 Pore size distribution (below 60 nm)

The cumulative pore size distributions (below 60 nm) of all samples are presented in Fig. 7 for 7, 14, 28, and 56 days of maturity, which provide the basis for several critical observations. It should be noted that nitrogen adsorption/desorption fails to quantitatively capture pore sizes around and greater than 60 nm [60–62], and discussions hereafter are as such, reflective of pore sizes smaller than the range. These pores are micropores and mesopores in hydrated cement paste as defined in [60]. The water to binder ratio of the pastes was 0.47 and at such level, the residual free water from cement hydration is expected to form coarser capillary pores [60, 83] that may not be captured in NAD isotherms [62]. However, the cumulative pore size distribution within the micro



◀ **Fig. 7** Temporal changes in the cumulative pore size distribution of **a** control, **b** FA, and **c** PGP mixes

and mesoporous region can still be evaluated qualitatively.

Figure 7a shows the gradual pore size transformation in hydrated cement paste over time. Between days 7 and 14, the volume of pores under 60 nm increased, due to the formation of small pores from the progressive filling of additional C–S–H gels in the void spaces from the ongoing hydration. The larger pores (> 60 nm) went through pore refinement and the volume of pores smaller than 60 nm increased. Between days 14 and 56, a volume reduction is observed of these pores, as identified by the curve progressively shifting downward. This indicates that the pore refinement of the control (100% cement) specimen was mostly achieved due to the fast reaction and continued hydration of cement in a steady-state condition, which may densify the cement matrix by reducing overall pore volumes of 10–60 nm. In essence, the larger pores (> 60 nm) transform to smaller ones and, with time, are further refined to result in lower pore volumes.

For FA incorporated paste in Fig. 7b, the temporal pore volume change is different from that observed for the control paste. Due to the dilution effect, the rate of hydration product formation and, consequently, the rate of pore refinement per unit volume of FA paste is expected to be slower than the control. Therefore, up to 28 days a slight, but gradual, refinement was marked by increasing volume of pores under 60 nm, likely from a higher degree of hydration for GP cement particles [62]. However, between 28 and 56 days, when cement hydration is slower, an increasing volume of micro and mesopores are still observed in Fig. 7b, and this appears to be associated with the pozzolanic reaction of the FA as identified in the TGA analysis. As such, the secondary hydration products due to the pozzolanic reaction continuously fill the larger capillary pores and, consequently, create the small or median capillary pores (< 60 nm).

The pore size transformation of PGP incorporated paste in Fig. 7c is different to that of control but somewhat like that of FA. The volume of pores below 60 nm steadily rises over time, preferably from the continuing refinement of pores over 60 nm size. As

per the case of FA paste (20 FA), the inclusion of the PGP led to a dilution effect, leading to the slower formation of hydration products (more porous matrix). With time, the large pores were continually being filled with hydration products from the hydration of cement. This may explain the observation that the volume of pores within 10–60 nm range did not drop, unlike in the control. Any contribution from the pozzolanic reaction cannot be confirmed for this pore refinement, as TGA analysis did not confirm PGP to consume CH; however, the latent hydraulic potential of PGP identified from the SAI test may contribute towards the gradual increase in the volume of pores below 60 nm size, due to the accumulation of additional reaction products from continued hydration. This is also evident in the heat release, where PGP offered relatively greater heat release than FA, likely from the combination of a higher number of nucleation sites and superior reactivity and thus a greater volume of larger than 60 nm pores.

### 3.5 Influence of recycled glass as fine aggregate

#### 3.5.1 Accelerated mortar bar tests (AMBT)

The mortar bar expansions for inclusion of glass aggregate at 20% and 40% were recorded up to 21 days (AS 1141.60.1 [64]) and 14 days (ASTM C1260 [63]) and the aggregates were classified following the AS and ASTM limits (Fig. 8a, b). The incorporation of glass as a replacement for sand facilitated ASR and causes measurable expansions in the mortar bar specimens. All aggregate proportions over 10% are ‘reactive’ as per AS and ‘potentially deleterious’ as per ASTM specifications. An aggregate mix containing 10% GFA and 90% of river sand is categorised as ‘slowly reactive’ as per AS or ‘uncertain’ as per ASTM. The expansion steadily increases with higher proportions of GFA as illustrated in Fig. 9.

There is a significant decline in expansion when cement is partially replaced with FA and PGP (mitigation series in Table 3) at 10 and 20%, as observed in Fig. 8c, d. The ASTM C1567 [19] was followed for the mitigation series, which allows the determination of the potential alkali-silica reactivity of combinations of cementitious materials and aggregate. A high potential for FA and PGP to limit ASR expansions was observed, with expansions of less than 0.10% after 14 days of conditioning were recorded for

all mixes and, as such, the aggregates in such systems were innocuous. At a higher SCM replacement of 20%, the expansions were lower, indicating the greater mitigation potential for higher SCM dosages. Moreover, mixes with FA demonstrated a relatively better potential for ASR mitigation than PGP. The role of FA and PGP in the mitigation of ASR expansion can be further discussed in the context of microstructural characterisations undertaken in this study.

Several mechanisms can contribute to the ASR mitigative potential of SCMs, including alkali dilution, alkali binding, reduced mass transport, consumption of portlandite in GP cement (thus, reducing pore solution pH), changes in pore solution chemistry, etc. [19, 39]. Although both FA and PGP were successful to keep ASR expansions within the limit (0.10%), their mechanisms may be different. It is recognised that AMBT conditions specimens at 80°C accelerates reactions of SCMs [28]. On the one hand, the data seems to be still relevant to specimens exposed to ambient conditions, despite the accelerated reactions at higher temperature, as the mechanism behind reduced expansions is similar [84–86]. On the other hand, the alkali contribution of SCMs on the alkalinity of the pore solution remains unclear, and is worthy of further investigation.

When replacing 20% cement with FA or PGP, there was an alkali and calcium dilution in the pore solution that, somewhat, restricts the process leading to damaging expansions. However, given that the specimens had continuous alkali supply from immersion in 1 mol/L NaOH solution throughout the test duration, this may not be the critical mechanism behind the expansion mitigation. FA demonstrated its ability to consume CH, making soluble calcium less available for the formation of expansive ASR gels; the presence of CH is critical for expansions due to ASR [19, 27]. Moreover, the pozzolanic reactivity of the FA means that the FA binds alkali and hydroxyl ions in the pore solution limiting their availability in ASR gel formation [22]. As a result, the efficiency of FA in expansion mitigation was marginally better than PGP. However, with a constant supply of alkalis in the AMBT test, the most critical mechanism is likely the limiting of mass transport from the inclusion of FA or PGP; both materials have taken part in pore refinement of large pores as suggested by the NAD analysis. This appears to limit the mass transport of alkalis from the 1 M NaOH solution. Although the contribution of

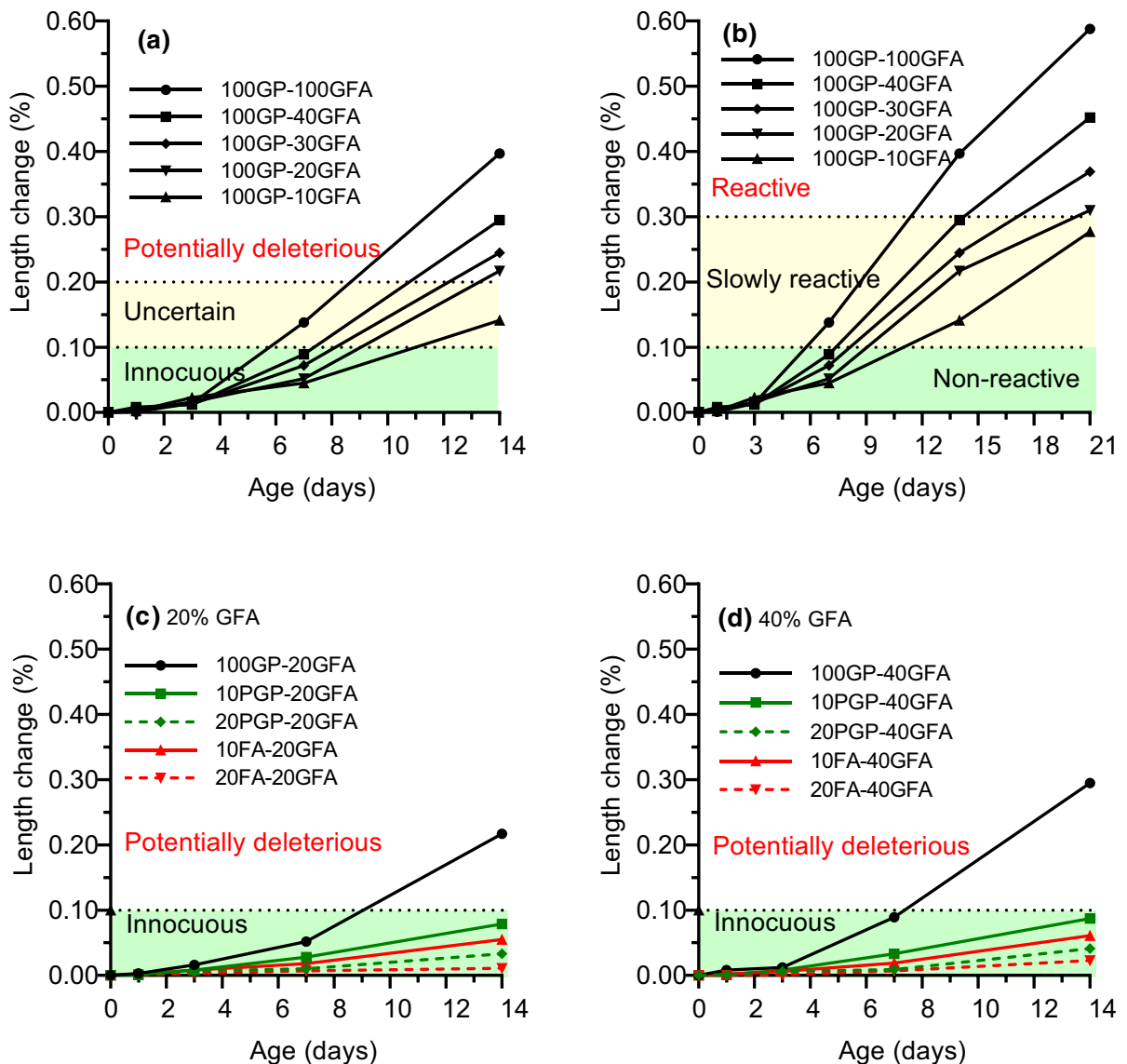


**Fig. 8** ASR expansion of mortar bars: **a** aggregate classification as per AS 1141.60.1; **b** aggregate classification as per - ASTM C1260; **c** mitigation of ASR expansion of 20% GFA

mortars using FA and PGP; **b** mitigation of ASR expansion of 40% GFA mortars using FA and PGP (notation details in Table 3)

the pozzolanic reactivity of FA was evident, the mechanism of PGP to some extent was unclear. However, its potential for ASR inhibition remains noteworthy. This may indicate that the amorphous silica of PGP (being several times finer than GFA) and its relatively high content of CaO may take part in both pozzolanic reactions and hydraulic reactions that can contribute to the formation of secondary C-S-H gels. The reactions may have been promoted at the temperature range of 80 °C adapted in the AMBT

test [87], limiting the expansions due to ASR within the acceptable limit of 0.10% as per ASTM 1567 [45]. Mirzahassemi and Riding [87] reported that glass powder does not demonstrate pozzolanic reactivity at 10 °C and 23 °C; however, at 50 °C, it consumes 17% CH in 28 days at a replacement level of 25%. At the 80 °C conditioning adopted in this study for the AMBT tests, both the FA and PGP demonstrated enhanced reactivity. As such, they take an active part in pore refinement and reduced the mobility of the



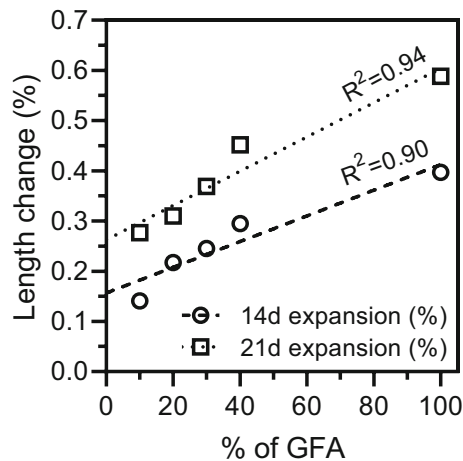


**Fig. 9** Correlation between proportion of GFA and expansion

alkalis, thus limiting ASR gel formation. For this reason, the ABMT samples with SCMs show a rare occurrence of ASR gels in their microstructure, which is discussed in the next section.

### 3.5.2 SEM–EDS analysis

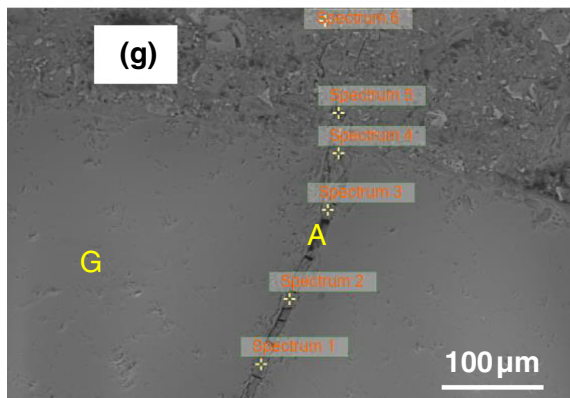
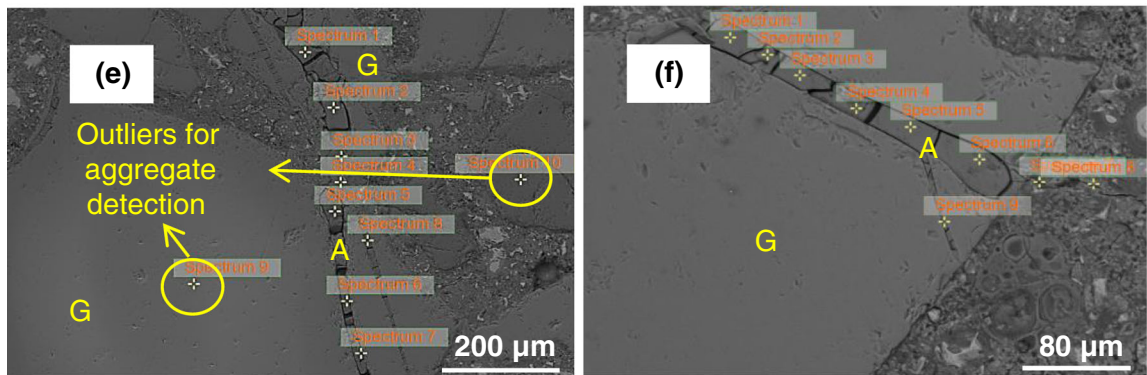
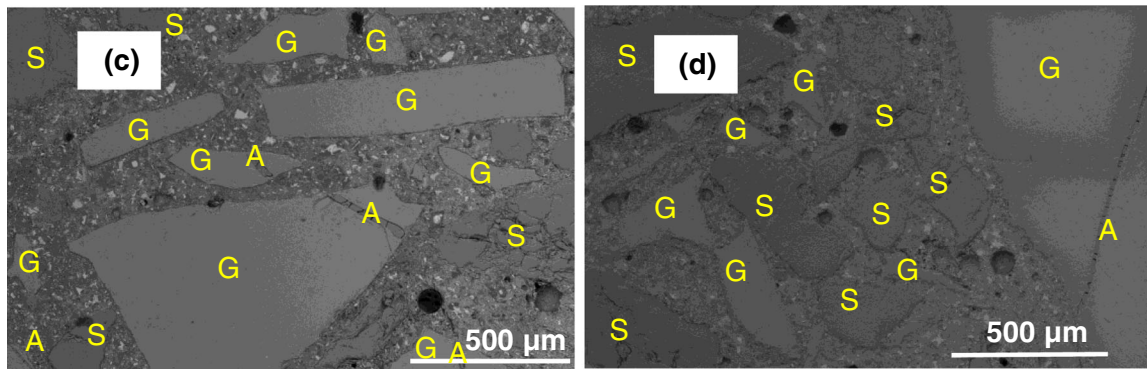
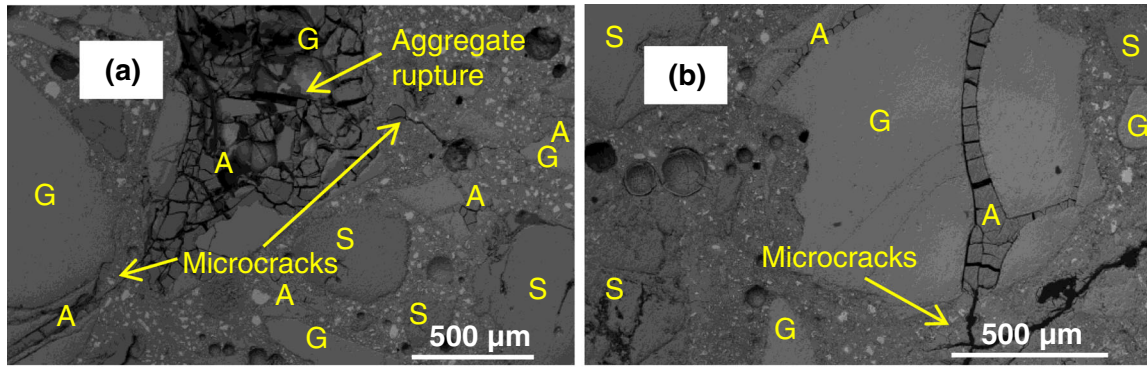
SEM imaging of the samples with and without SCMs were undertaken to identify changes in morphological features, enabling qualitative identification of ASR gels. EDS analysis was also undertaken to observe if the presence of FA and PGP alter the chemical composition of the ASR gels. The SEM images present a clear distinction between the control specimens (Fig. 10a, b) to those with 10% FA (Fig. 10c) and 10% PGP (Fig. 10d) after 14 days of exposure to 1 mol/L NaOH solution at 80 °C as per ASTM C1567 [45]. The control specimen was severely damaged with a large volume of ASR gel formation within the glass aggregates, often to an extent causing total disruption of the aggregate particle (Fig. 10a). The swelling of the ASR gels in the control specimen also led to the formation of microcracks within the matrix, severely damaging the integrity of the specimens. Extensive cracking of the mortar prisms was also visually observed in some specimens. To the contrary, with the substitution of 10% cement with FA or PGP, the occurrence of ASR gel was significantly reduced. Only a trace amount of ASR gel is observed in Fig. 10c, d, with several glass aggregates showing no indication of gel formation. The ASR gel thickness formed in the control specimens range from 50 to

500 μm; whereas, in the SCM specimens, the gel thickness reduced to about 2–5 μm, meaning the gel did not swell sufficiently to cause microcracking. The microstructure corroborates the expansion readings of Fig. 8c, d, where a significant reduction is achieved with SCM substitution.

Approximate Ca/Si and (Na + K)/Si ratios were measured based on EDS analysis on ASR gels formed within the glass particles, and in the microcracks, in the vicinity of glass particles. Figure 10e–g show representative locations where EDS analysis was undertaken; not all images have been included in this paper. The results of elemental analysis are summarised in Table 5. Mirzahosseini and Riding [88, 89] and Afshinnia and Rangaraju [88, 89] report that ASR gels initially form in the cracks within glass particles (cracks originating from the mechanical crushing of recycled glass) before expanding through the microcracks within the matrix around the glass particle and progressively inducing damage. Assessment of the elemental compositions demonstrates that the composition of ASR gel was location-dependent but not dependent on the binder composition [90]. The results also suggest that the reactive silica from the amorphous FA, and the PGP, likely contribute to reaction product formations, rather than in ASR gel formations, unlike species from the GFA.

The Ca/Si ratio measured on ASR gels within glass particles was of the range of 0.23–0.26, characterising typical gel compositions in alkali-reactive aggregates [10, 90, 91]. However, the Ca/Si ratio of ASR gel measured within microcracks along the interfacial transition zone (ITZ) was 0.56. This change in the elemental ratio confirms that the composition of the gel is location dependent. Also, the Ca/Si ratio measured within the cracks was much lower than the typical Ca/Si of a neat Portland cement paste (~ 1.75) [92]. This obvious difference suggests that the locations chosen for the elemental analysis are indeed ASR gels rich in alkali and Si, and low in Ca, that have propagated in the microcracks around the glass aggregates [93]. The increased Ca/Si ratio in the matrix, compared to within GFA, is linked to alkali recycling due to the calcium replacement of ASR gels [94]. Similar findings with higher Ca/Si ratio are reported in [90, 91, 95, 96].

The Ca/Si ratio of ASR gels in the FA and PGP incorporated mixes were similar to that of the control, with no appreciable difference in composition. This





◀ **Fig. 10** SEM images of mortars investigated in this study: **a, b** 100GP-40GFA; **c** 10FA-40GFA; **d** 10PGP-40GFA; **e** point locations for EDS analysis of 100GP-40GFA; **f** point locations for EDS analysis of 10FA-40GFA; **g** point locations for EDS analysis of 10FA-40GFA. Notations in the figure are *G* Glass fine aggregate (GFA); *S* River sand; and *A* ASR gel. Sample IDs are available in Table 3

comparable composition of the ASR gel in the control and SCM specimens indicates that neither FA or PGP necessarily alter ASR gel composition [19]. Thus, it is not the nature of the ASR gel that dictates the reduced expansion, rather the substantial reduction of ASR gel formation, in contrast to the control specimens, that leads to the reduced expansion recorded in the AMBT test. SCMs limit the unfavourable conditions for a damaging level of ASR gel formation, such as high alkali content in the pore solution, the availability of reactive silica, and easy access for ion transport, etc. They do not necessarily alter the chemistry of the ASR gel towards reduced expansion.

#### 4 Conclusions

This research investigates the (1) reactivity and (2) ASR mitigation potential of PGP as a SCM and compares its performance against similar substitution using low-calcium FA. Finely ground glass powder can be utilised as a potential SCM that can contribute to better strength gain than FA with similar ASR mitigation potential. The results of this study validate the use of pulverised glass powder, as an ASR mitigator, together with use of recycled glass aggregate in cementitious composites. The key findings of this study are summarised below:

- Fine PGP of median particle size of 19.3  $\mu\text{m}$  enhances strength gain towards achieving a strength activity index (SAI) of over 75%. The SAI of FA at 7 and 28 days are 66% and 71%,

respectively. PGP with a median particle size of 80.9  $\mu\text{m}$  reaches SAI of 53 and 55% in 7 and 28 days, confirming the fineness of glass powder to be a critical factor for strength gain.

- The higher heat released per unit mass of cement confirms the filler effect of both FA and PGP. The effect is more prominent at higher levels of replacement, leading to greater heat release. PGP results in higher heat releases per gram of cement than FA in the first three days of hydration, possibly due to a higher volume of pores over 60 nm in size. The heat released per unit mass of binder also indicates a likely hydraulic reactivity of PGP. The occurrence of the acceleration peak in the heat flow curve is delayed by 30 min and 50 min for the inclusion of 20% FA and PGP, respectively.
- FA continually consumes CH of hydrated cement paste, whereas PGP does not demonstrate any CH consumption. Despite this lack of pozzolanic reactivity of PGP, the significant strength gain it offered in the SAI test indicates latent hydraulic properties.
- Both FA and PGP transform the distribution of pore size below 60 nm by continually filling up larger pores. The changes in the pore size distribution are related to the pozzolanic reactivity of FA and the apparent hydraulic reactivity of PGP. Regardless, the volume of pores in the 10–60 nm range is relatively higher for PGP.
- The use of PGP at 10% and above can effectively suppress the expansion of a composite with up to 40% glass fine aggregate (GFA) within the standardised acceptable limit of 0.10%. The potential of PGP as an ASR inhibitor is comparable to FA, with the latter providing a slightly better performance possibly owing to its pozzolanic reactions (CH consumption) and a relatively lower pore volume in the micro and mesopore range.
- The inclusion of PGP improves the microstructure of GFA mortars by limiting the formation of ASR

**Table 5** Elemental ratios determined by EDS on locations of interest

Mix ID	Location	No. of points	Avg. Ca/Si	Avg. (Na + K)/Si
100GP-40GFA	ASR gel	35	0.26 $\pm$ 0.06	0.33 $\pm$ 0.09
10FA-40GFA	ASR gel	28	0.20 $\pm$ 0.03	0.41 $\pm$ 0.09
10 PGP-40GFA	ASR gel	43	0.23 $\pm$ 0.08	0.36 $\pm$ 0.08
100GP-40GFA	Near ITZ	13	0.56 $\pm$ 0.04	0.44 $\pm$ 0.07

gels through a coupled action of reduced mass transport from pore refinement and alkali dilution. FA does this more effectively from the added mechanism of CH consumption.

- The inclusion of FA or PGP does not alter the ASR gel composition of GFA. However, as observed in SEM images and expansion measurements, they strongly mitigate the ASR gel formation by controlling the critical parameters necessary for damaging ASR gels to occur.

**Acknowledgements** The authors acknowledge Centre for Infrastructure Engineering and Safety (CIES) for supporting laboratory resources. The authors also acknowledge the instruments of Microscopy Australia at the Mark Wainwright Analytical Centre, University of New South Wales, a facility that is funded by the University, and State and Federal Governments.

**Funding** Open Access funding enabled and organized by CAUL and its Member Institutions. Partial financial support was received from XL I-Mix Pty Ltd and the Department of Industry, Science, Energy, and Resources of Australian Government.

#### Declarations

**Conflict of interest** The authors have no competing interests to declare that are relevant to the content of this article.

**Open Access** This article is licensed under a Creative Commons Attribution 4.0 International License, which permits use, sharing, adaptation, distribution and reproduction in any medium or format, as long as you give appropriate credit to the original author(s) and the source, provide a link to the Creative Commons licence, and indicate if changes were made. The images or other third party material in this article are included in the article's Creative Commons licence, unless indicated otherwise in a credit line to the material. If material is not included in the article's Creative Commons licence and your intended use is not permitted by statutory regulation or exceeds the permitted use, you will need to obtain permission directly from the copyright holder. To view a copy of this licence, visit <http://creativecommons.org/licenses/by/4.0/>.

#### References

1. Analysis of Australia's municipal recycling infrastructure capacity. October 2018.
2. Kashani A, Ngo TD, Hajimohammadi A (2019) Effect of recycled glass fines on mechanical and durability properties of concrete foam in comparison with traditional cementitious fines. *Cement Concr Compos* 99:120–129
3. Hajimohammadi A, Ngo T, Kashani A (2018) Glass waste versus sand as aggregates: the characteristics of the evolving geopolymer binders. *J Clean Prod* 193:593–603
4. Hajimohammadi A, Ngo T, Kashani A (2018) Sustainable one-part geopolymer foams with glass fines versus sand as aggregates. *Constr Build Mater* 171:223–231
5. Schmidt A, Saia W (1963) Alkali-aggregate reaction tests on glass used for exposed aggregate wall panel work. *ACI Mater J* 60:1235–1236
6. Visser JHM (2018) Fundamentals of alkali-silica gel formation and swelling: condensation under influence of dissolved salts. *Cem Concr Res* 105:18–30
7. Rajabipour F, Giannini E, Dunant C et al (2015) Alkali-silica reaction: current understanding of the reaction mechanisms and the knowledge gaps. *Cem Concr Res* 76:130–146
8. Kim T, Alnahhal MF, Nguyen QD et al (2019) Initial sequence for alkali-silica reaction: Transport barrier and spatial distribution of reaction products. *Cement Concr Compos* 104:103378
9. Leemann A, Le Saout G, Winnefeld F et al (2011) Alkali-silica reaction: the influence of calcium on silica dissolution and the formation of reaction products. *J Am Ceram Soc* 94(4):1243–1249
10. Kim T, Olek J (2014) Chemical sequence and kinetics of alkali-silica reaction part I. *Experiments* 97(7):2195–2203
11. Struble LJ, Diamond S (1981) Swelling properties of synthetic alkali silica gels. *J Am Ceram Soc* 64(11):652–655
12. Shafaatian S (2012) Innovative methods to mitigate alkali-silica reaction in concrete materials containing recycled glass aggregates. Ph. D. Dissertation, Pennsylvania State University.
13. Kim T, Olek J, Jeong H (2015) Alkali-silica reaction: kinetics of chemistry of pore solution and calcium hydroxide content in cementitious system. *Cem Concr Res* 71:36–45
14. Bulteel D, Garcia-Diaz E, Vernet C et al (2002) Alkali-silica reaction: a method to quantify the reaction degree. *Cem Concr Res* 32(8):1199–1206
15. Kim T, Olek J (2014) Chemical sequence and kinetics of alkali-silica reaction part II. A thermodynamic model. *J Am Ceram Soc* 97(7):2204–2212
16. Hou X, Struble LJ, Kirkpatrick RJ (2004) Formation of ASR gel and the roles of C-S-H and portlandite. *Cem Concr Res* 34(9):1683–1696
17. Rangaraju PR, Desai J (2009) Effectiveness of fly ash and slag in mitigating alkali-silica reaction induced by deicing chemicals. *J Mater Civ Eng* 21(1):19–31
18. Aquino W, Lange DA, Olek J (2001) The influence of metakaolin and silica fume on the chemistry of alkali-silica reaction products. *Cement Concr Compos* 23(6):485–493
19. Shafaatian SMH, Akhavan A, Maraghechi H et al (2013) How does fly ash mitigate alkali-silica reaction (ASR) in accelerated mortar bar test (ASTM C1567)? *Cement Concr Compos* 37:143–153
20. Moser RD, Jayapalan AR, Garas VY et al (2010) Assessment of binary and ternary blends of metakaolin and Class C fly ash for alkali-silica reaction mitigation in concrete. *Cem Concr Res* 40(12):1664–1672
21. Hay R, Ostertag CP (2021) New insights into the role of fly ash in mitigating alkali-silica reaction (ASR) in concrete. *Cem Concr Res* 144:106440
22. Duchesne J, Bérubé M (1994) Effectiveness of supplementary cementing materials in suppressing expansion due



- to ASR: part 2. Effect on the pore solution chemistry. *Cem Concr Res* 24:221–230
23. Canham I, Page C, Nixon P (1987) Aspects of the pore solution chemistry of blended cements related to the control of alkali silica reaction. *Cem Concr Res* 17(5):839–844
  24. Diamond S (1981) Effects of two Danish fly ashes on alkali contents of pore solutions of cement-flyash pastes. *Cem Concr Res* 11(3):383–394
  25. Hobbs D (1982) Influence of pulverized-fuel ash and granulated blastfurnace slag upon expansion caused by the alkali-silica reaction. *Mag Concr Res* 34(119):83–94
  26. Chatterji S (1979) The role of  $\text{Ca}(\text{OH})_2$  in the breakdown of Portland cement concrete due to alkali-silica reaction. *Cem Concr Res* 9(2):185–188
  27. Bleszynski RF, Thomas MD (1998) Microstructural studies of alkali-silica reaction in fly ash concrete immersed in alkaline solutions. *Adv Cem Based Mater* 7(2):66–78
  28. Lothenbach B, Scrivener K, Hooton R (2011) Supplementary cementitious materials. *Cem Concr Res* 41(12):1244–1256
  29. American Coal Ash Association (ACAA) 2017 production and use charts.
  30. Fanijo EO, Kassem E, Ibrahim A (2021) ASR mitigation using binary and ternary blends with waste glass powder. *Constr Build Mater* 280:122425
  31. Afshinnia K, Rangaraju PR (2015) Efficiency of ternary blends containing fine glass powder in mitigating alkali-silica reaction. *Constr Build Mater* 100:234–245
  32. Cai Y, Xuan D, Poon CS (2019) Effects of nano- $\text{SiO}_2$  and glass powder on mitigating alkali-silica reaction of cement glass mortars. *Constr Build Mater* 201:295–302
  33. Ke G, Li W, Li R et al (2018) Mitigation effect of waste glass powders on alkali-silica reaction (ASR) expansion in cementitious composite. *Int J Concr Struct Mater* 12(1):67
  34. Zheng K (2016) Pozzolanic reaction of glass powder and its role in controlling alkali-silica reaction. *Cement Concr Compos* 67:30–38
  35. Afshinnia K, Rangaraju PR (2015) Mitigating alkali-silica reaction in concrete: effectiveness of ground glass powder from recycled glass. *Transp Res Recod* 2508(1):65–72
  36. Ichikawa T (2009) Alkali-silica reaction, pessimum effects and pozzolanic effect. *Cem Concr Res* 39(8):716–726
  37. Zhang C, Wang A, Tang M et al (1999) Influence of aggregate size and aggregate size grading on ASR expansion. *Cem Concr Res* 29(9):1393–1396
  38. Jin W, Meyer C, Baxter S (2000) “Glascrete”-concrete with glass aggregate. *ACI Mater J* 97(2):208–213
  39. Taha B, Nounu G (2008) Using lithium nitrate and pozzolanic glass powder in concrete as ASR suppressors. *Cement Concr Compos* 30(6):497–505
  40. ASTM C131 Standard test method for resistance to degradation of small-size coarse aggregate by abrasion resistance and impact in the Los Angeles machine (2006). ASTM International, West Conshohocken, PA
  41. Dyer TD, Dhir RK (2001) Chemical reactions of glass cullet used as cement component. *J Mater Civil Eng* 13(6):412–417
  42. Ramadan M, El-Gamal SMA, Selim FA (2020) Mechanical properties, radiation mitigation and fire resistance of OPC-recycled glass powder composites containing nanoparticles. *Constr Build Mater* 251:118703
  43. Jang H, Jeon S, So H et al (2015) Properties of different particle size of recycled TFT-LCD waste glass powder as a cement concrete binder. *Int J Precis Eng Manuf* 16(12):2591–2597
  44. Aliabdo AA, Abd Elmoaty AEM, Aboshama AY (2016) Utilization of waste glass powder in the production of cement and concrete. *Constr Build Mater* 124:866–877
  45. ASTM C1567-13 Standard test method for determining the potential alkali-silica reactivity of combinations of cementitious materials and aggregate (accelerated mortar-bar method) (2013). ASTM International, West Conshohocken, PA
  46. AS 3972 General purpose and blended cements (2010). Standards Australia
  47. AS 3582.1 Supplementary cementitious materials Part 1: fly ash (2016). Standards Australia.
  48. ASTM C188-17 Standard test method for density of hydraulic cement (2017). ASTM International, West Conshohocken, PA
  49. Ward CR, French D (2006) Determination of glass content and estimation of glass composition in fly ash using quantitative X-ray diffractometry. *Fuel* 85(16):2268–2277
  50. AS 1141.35 Methods for sampling and testing aggregates Sugar (2007). Standards Australia.
  51. AS 1141.5 Methods for sampling and testing aggregates—particle density and water absorption of fine aggregate (2000). Standards Australia
  52. ASTM C311 / C311M-18 standard test methods for sampling and testing fly ash or natural pozzolans for use in Portland-cement concrete (2018). ASTM International, West Conshohocken, PA
  53. Snellings R, Chwast J, Cizer Ö et al (2018) RILEM TC-238 SCM recommendation on hydration stoppage by solvent exchange for the study of hydrate assemblages. *Mater Struct* 51(6):172
  54. Zhang Z, Scherer GW (2021) Physical and chemical effects of isopropanol exchange in cement-based materials. *Cem Concr Res* 145:106461
  55. Kim T, Olek J (2012) Effects of sample preparation and interpretation of thermogravimetric curves on calcium hydroxide in hydrated pastes and mortars. *Transp Res Rec* 2290(1):10–18
  56. Scrivener K, Snellings R, Lothenbach B (2018) A practical guide to microstructural analysis of cementitious materials. CRC Press, Boca Raton
  57. Barrett EP, Joyner LG, Halenda PP (1951) The determination of pore volume and area distributions in porous substances. I. Computations from nitrogen isotherms. *J Am Chem Soc* 73(1):373–380
  58. Kaufmann J, Loser R, Leemann A (2009) Analysis of cement-bonded materials by multi-cycle mercury intrusion and nitrogen sorption. *J Colloid Interface Sci* 336(2):730–737
  59. Cychosz KA, Guillet-Nicolas R, García-Martínez J et al (2017) Recent advances in the textural characterization of hierarchically structured nanoporous materials. *Chem Soc Rev* 46(2):389–414
  60. Zeng Q, Li K, Fen-Chong T et al (2016) Pore structure of cement pastes through NAD and MIP analysis. *Adv Cem Res* 28(1):23–32

61. Aligizaki KK (2004) Pore structure of cement-based materials—testing, interpretation and requirements. CRC Press, London
62. Zeng Q, Li K, Fen-chong T et al (2012) Pore structure characterization of cement pastes blended with high-volume fly-ash. *Cem Concr Res* 42(1):194–204
63. ASTM C1260-14 Standard test method for potential alkali reactivity of aggregates (mortar-bar method) (2014). ASTM International, West Conshohocken, PA
64. AS 1141.60.1 Methods for sampling and testing aggregates—potential alkali-silica reactivity—accelerated mortar bar method (2014). Standards Australia.
65. ASTM C618-15 Standard specification for coal fly ash and raw or calcined natural pozzolan for use in concrete (2015). ASTM International, West Conshohocken, PA
66. Huang L, Yan P (2019) Effect of alkali content in cement on its hydration kinetics and mechanical properties. *Constr Build Mater* 228:116833
67. Carette GG, Malhotra VM (1987) Characterization of Canadian fly ashes and their relative performance in concrete. *Can J Civil Eng* 14(5):667–682
68. Das SK, Yudhbir A (2006) simplified model for prediction of pozzolanic characteristics of fly ash, based on chemical composition. *Cem Concr Res* 36(10):1827–1832
69. Dhir RK, Munday JGL, Ong LT (1981) Strength variability of OPC/PFA concrete. *Concrete* 15(6):33–37
70. Krstic M, Davalos JF (2019) Field application of recycled glass pozzolan for concrete. *ACI Mater J* 116(4):123–131
71. Nassar R-U-D, Soroushian P (2012) Strength and durability of recycled aggregate concrete containing milled glass as partial replacement for cement. *Constr Build Mater* 29:368–377
72. Pourkhorshidi AR, Najimi M, Parhizkar T et al (2010) Applicability of the standard specifications of ASTM C618 for evaluation of natural pozzolans. *Cement Concr Compos* 32(10):794–800
73. Gartner E, Young J, Damidot D, et al (2002) Hydration of Portland cement. In: *Structure and performance of cements*. CRC Press, Boca Raton, pp 57–108
74. Bullard JW, Jennings HM, Livingston RA et al (2011) Mechanisms of cement hydration. *Cem Concr Res* 41(12):1208–1223
75. Ylmén R, Wadsö L, Panas I (2010) Insights into early hydration of Portland limestone cement from infrared spectroscopy and isothermal calorimetry. *Cem Concr Res* 40(10):1541–1546
76. Vollet DR, Craievich AF (2000) Effects of temperature and of the addition of accelerating and retarding agents on the kinetics of hydration of tricalcium silicate. *J Phys Chem B* 104(51):12143–12148
77. Hjorth J, Skibsted J, Jakobsen HJ (1988) <sup>29</sup>Si MAS NMR studies of Portland cement components and effects of microsilica on the hydration reaction. *Cem Concr Res* 18(5):789–798
78. Narmluk M, Nawa T (2011) Effect of fly ash on the kinetics of Portland cement hydration at different curing temperatures. *Cem Concr Res* 41(6):579–589
79. Fajun W, Grutzeck MW, Roy DM (1985) The retarding effects of fly ash upon the hydration of cement pastes: the first 24 hours. *Cem Concr Res* 15(1):174–184
80. Afroz S, Zhang Y, Nguyen QD et al (2022) Effect of limestone in general purpose cement on autogenous shrinkage of high strength GGBFS concrete and pastes. *Constr Build Mater* 327:126949
81. De Weerd K, Haha MB, Le Saout G et al (2011) Hydration mechanisms of ternary Portland cements containing limestone powder and fly ash. *Cem Concr Res* 41(3):279–291
82. Suraneni P, Hajibabae A, Ramanathan S et al (2019) New insights from reactivity testing of supplementary cementitious materials. *Cem Concr Compos* 103:331–338
83. Chen X, Wu S (2013) Influence of water-to-cement ratio and curing period on pore structure of cement mortar. *Constr Build Mater* 38:804–812
84. Thomas MDA, Fournier B, Folliard K et al (2007) Performance limits for evaluating supplementary cementing materials using accelerated mortar bar tests. *ACI Mater J* 104(2):115–122
85. Tapas MJ, Thomas P, Vessalas K et al (2022) Mechanisms of alkali-silica reaction mitigation in AMBT conditions: comparative study of traditional supplementary cementitious materials. *J Mater Civil Eng* 34(3):04021460
86. Shayan A, Xu A (2004) Value-added utilisation of waste glass in concrete. *Cem Concr Res* 34(1):81–89
87. Mirzahosseini M, Riding KA (2015) Influence of different particle sizes on reactivity of finely ground glass as supplementary cementitious material (SCM). *Cement Concr Compos* 56:95–105
88. Maraghechi H, Shafaatian S-M-H, Fischer G et al (2012) The role of residual cracks on alkali silica reactivity of recycled glass aggregates. *Cement Concr Compos* 34(1):41–47
89. Afshinnia K, Rangaraju PR (2015) Influence of fineness of ground recycled glass on mitigation of alkali-silica reaction in mortars. *Constr Build Mater* 81:257–267
90. Thaulow N, Jakobsen UH, Clark B (1996) Composition of alkali silica gel and ettringite in concrete railroad ties: SEM-EDX and X-ray diffraction analyses. *Cem Concr Res* 26(2):309–318
91. Knudsen T, Thaulow N (1975) Quantitative microanalyses of alkali-silica gel in concrete. *Cem Concr Res* 5(5):443–454
92. Richardson IG (1999) The nature of C-S-H in hardened cements. *Cem Concr Res* 29(8):1131–1147
93. Lu J-X, Zhan B-J, Duan Z-H et al (2017) Improving the performance of architectural mortar containing 100% recycled glass aggregates by using SCMs. *Constr Build Mater* 153:975–985
94. Thomas M (2001) The role of calcium hydroxide in alkali recycling in concrete. *Mater Sci Concr Spec* 460:225–236
95. Katayama T (2012) ASR gels and their crystalline phases in concrete—universal products in alkali-silica, alkali-silicate and alkali-carbonate reactions. In: *Proc 14th int conf alkali aggreg react (ICAAR)*, Austin, Texas
96. Katayama T (1998) Petrographic diagnosis of alkali-aggregate reaction in concrete based on quantitative EPMA analysis. *ACI Symposium Publication*, p 179

**Publisher's Note** Springer Nature remains neutral with regard to jurisdictional claims in published maps and institutional affiliations.

